photonics

MDPI

Article

In-Situ Temporal Characterization of Chirped Ultra-Broadband Laser Pulses Exciting a Dual-Light Emitter Er^{3+}-Doped Perovskite

Óscar Pérez-Benito and Rosa Weigand *

Department of Optics, Faculty of Physics, Universidad Complutense de Madrid, Plaza de Ciencias 1, 28040 Madrid, Spain; oscper03@ucm.es

* Correspondence: weigand@fis.ucm.es

Abstract: We take advantage of the dual emission properties of up-conversion fluorescence (UCF) and second harmonic generation (SHG) in Er^{3+}-doped perovskite $Na_{0.95}Er_{0.05}Nb_{0.9}Ti_{0.1}O_3$ to fully temporally characterize the ultrashort laser pulse that excites Er^{3+}-ion fluorescence. The chirped pulses from a broadband Ti:Sa oscillator are temporally characterized using the dispersion scan (d-scan) technique by using the SHG signal in the host perovskite at the same point where UCF is being produced by the same pulse. The pulse durations obtained range from ~45 fs to ~8 fs and positive and negative spectral phases are unambiguously identified. The temporal characterization is compared using a standard non-linear crystal and perfect agreement is obtained. These results show that it is possible to temporally characterize in-situ ultrashort laser pulses while they are inducing a UCF process, as long as the host generates second-harmonic signal.

Keywords: second harmonic generation; up-conversion fluorescence; perovskites; ultrashort pulse measurement

1. Introduction

Particles with emission in different spectral ranges are interesting for a variety of research fields, such as bioimaging and photodynamic therapy [1–4]. A successful system combines fluorescence emission obtained in a rare-earth ion with the signal obtained by second harmonic generation (SHG). Core-shell systems such as KTP@$LaPO_4$:Eu nanoparticles have exhibited simultaneous SHG and up-conversion fluorescence (UCF) but each signal was excited by a different laser. In particular, an ultrafast Titanium:Sapphire (Ti:Sa) oscillator was used to produce SHG in KTP and a continuous-wave laser operating at 532 nm was used to excite the Eu fluorescence [5]. The use of a single laser is also possible for some systems such as erbium-doped α-$La_{0.85}Er_{0.15}(IO_3)_3$ [6]. In particular, a laser operating at 980 nm simultaneously produced SHG and up-conversion fluorescence. The same was observed using a laser operating at 800 nm.

Recently we synthesized nano and micrometer-sized particles [7] of an Er^{3+}-doped perovskite ($Na_{0.95}Er_{0.05}Nb_{0.9}Ti_{0.1}O_3$), which showed a dual emission behavior when excited by ultrashort laser pulses from a single Ti:Sa broadband oscillator. The laser had a broad-band emission from 650 to 1000 nm. On one side the laser spectrum included the wavelengths 790 nm and 980 nm. Those wavelengths excited the Er^{3+} ion by an up-conversion process and the fluorescence exhibited its characteristic green emission in the range 500–580 nm. The excitation and emission processes are represented in Figure 1 in a simplified scheme. On the other side, the host displayed second-harmonic generation in the range 360–440 nm. The intensity of the green fluorescence bands scaled with the laser intensity as $I^{1.69}$, while the SHG signal scaled as $I^{1.99}$. Moreover, the fluorescence and SHG spectra were recorded as a function of the dispersion introduced by a variable dispersion compressor, composed of a pair of mobile glass wedges and a pair of chirped mirrors (with a fixed number of bounces). The spectra of both systems changed with the dispersion added to the pulse, i.e., the generated SHG or UCF signals were sensitive to the chirp of the pulses.

check for updates

Citation: Pérez-Benito, Ó.; Weigand, R. In-Situ Temporal Characterization of Chirped Ultra-Broadband Laser Pulses Exciting a Dual-Light Emitter Er^{3+}-Doped Perovskite. *Photonics* **2023**, *10*, 947. https://doi.org/10.3390/photonics10080947

Received: 24 July 2023
Revised: 7 August 2023
Accepted: 14 August 2023
Published: 18 August 2023

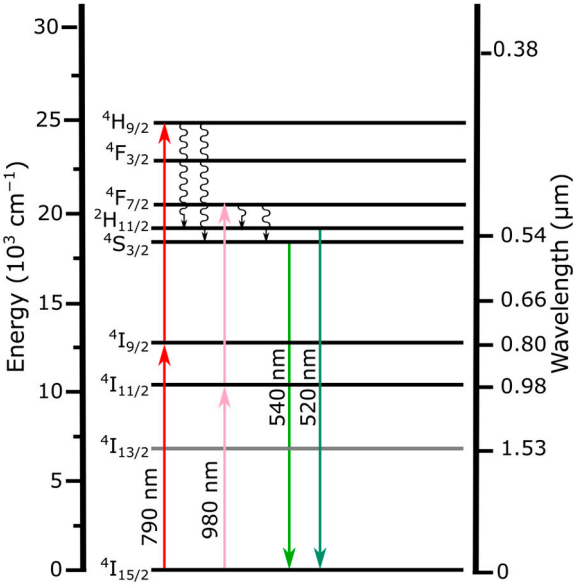

Figure 1. Simplified scheme of energy levels of Er^{3+}.

The dependence of fluorescence emission on the pulse chirp has been studied in different systems, and both an increase and decrease in the fluorescence intensity depending on the material have been observed. An increase of up to 5–6 times of the autofluorescence generated in NPC cells (Nasopharyngeal carcinoma cells) with compressed pulses has been reported [8]. Studies performed in chromophores in liquid phase have shown an enhancement of the fluorescence with the linear chirp, before pulse broadening was large enough to reduce the fluorescence intensity [9]. In gases, chirp effects in the 3-photon absorption yields of molecular iodine have been observed, with a factor of 3 enhancement for chirped pulses compared to transform-limited chirp-free pulses [10]. In general, since shorter pulses are more intense than longer pulses provided they carry the same energy, an increase of fluorescence intensity is expected when using compressed pulses compared to chirped and longer pulses. However, if coherent processes are present in the system under study, the effects induced by the chirp can dominate over the pulse duration. In particular, in $Na_{0.95}Er_{0.05}Nb_{0.9}Ti_{0.1}O_3$ we observed a depletion in the fluorescence for compressed pulses, while fluorescence increased for positively or negatively chirped pulses. The increase was larger for negatively chirped pulses compared to positively chirped pulses. We demonstrated that this behavior was due to quantum interference effects among several levels of Er^{3+} [7].

In the case of SHG, the sensitivity of the generated spectrum to the chirp of the pulses has been applied to the measurement of broadband laser pulses, a technique which is called dispersion scan (d-scan). The basis of this technique is the acquisition of traces consisting of different SHG spectra in function of known dispersion values (applied by a variable dispersion compressor) [11,12]. From these measurements one can extract, by using a proper algorithm, the spectral phase and intensity of the pulse for every configuration of the variable dispersion compressor. Details about d-scan are given in the Materials and Methods section. This technique can be implemented using bulk crystals [11,12] and also micro- and nano-crystals [13,14]. In [13] we demonstrated that it is also possible to temporally characterize ultrashort laser pulses using SHG produced in $BaTiO_3$ nanoparticles. The d-scan traces were slightly different to the traces generated in bulk BBO (Beta Barium Borate) crystal. This was not only due to the different nonlinear response of both systems, but also because of light scattering that affected the laser pulses and the SHG signal, as the light interacted with a system which does not have bulk features, but rather features associated to a discretized system composed of nanoparticles. The retrieval algorithm had to be extended in order to account for the scattering effects. Perfect agreement was then obtained between the temporal characterization done with the BBO crystal and the one

done with the $BaTiO_3$ nanoparticles [13]. Recently, we have demonstrated that this behavior has a universal character, and clusters of micro- or nano-sized particles can be used to temporally characterize few-cycle laser pulses using the d-scan technique, independently of their size and the composition of the particles, as long as they generate SHG [14]. This is due to the fact that for small-sized crystals with a $\chi^{(2)}$ response, the shape of the SH spectra changes with the chirp of the pulses, as required by the d-scan technique. If more or less particles participate in the SHG, this will affect the intensity of the total signal, but the dependence of the SH spectrum on the pulse chirp will still be present.

In this paper we show that the SHG signal of the nano and micrometer-sized particles of the Er^{3+}-doped perovskite host can be used to in-situ temporally characterize the pulse which is interacting with the Er^{3+} ions, without the need for an additional bulk crystal.

2. Materials and Methods

Er^{3+}-doped perovskite synthesis by the hydrothermal method and the corresponding characterization through electron microscopy is described elsewhere, in [7]. The non-centrosymmetric $P2_1ma$ space group for the $Na_{0.95}Er_{0.05}Nb_{0.9}Ti_{0.1}O_3$ perovskite was determined by X-ray diffraction [7] (See also Appendix A, provided as supplementary material). Notice that the host has to be non-centrosymmetric in order to generate SHG. The dopant content and its location in the host crystal structure were studied by XEDS (energy-dispersive X-ray spectroscopy) and HAADF STEM imaging (high-angle annular dark-field scanning transmission electron microscope), respectively. The synthesized particles (Ps) have a broad size distribution ranging from nano to micrometer sizes. A dispersion of the particles in n-butanol is sonicated for 15 min. Using a micropipette, 2 µL drops are taken from the supernatant and deposited on a microscope coverslip (150 µm-thick). The number of drops is chosen so that the linear transmittance of the samples is around 50% (as measured with a Titanium:Sapphire oscillator in continuous wave). The appearance of the samples can be seen in Figure 2 as taken with a camera (Figure 2a), an optical microscope (Figure 2b) and a Scanning Electron Microscope (SEM image, Figure 2c). The particles are uniformly distributed over the substrate; the discrete nature of the sample can be easily seen and they are polydisperse.

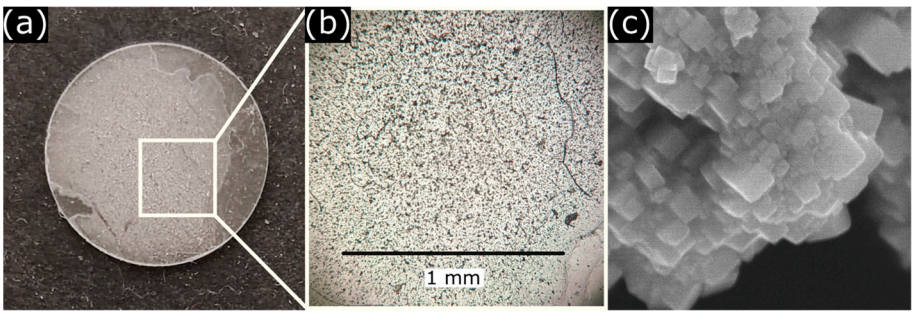

Figure 2. Optical image of the sample taken with a camera (**a**), with an optical microscope (**b**) and image taken with a Scanning Electron Microscope (**c**).

We employ a home-made Titanium: Sapphire oscillator (10 fs, 80 MHz, 60 mW average power). The spectrum of the laser is broadband and can be seen in Figure 3. It covers a range between 650 and 1000 nm. It has some structure, with bands peaked at 766 nm and 980 nm. This means that the laser can excite upper levels of Er^{3+} by an up-conversion process. The laser pulses pass through a variable dispersion compressor consisting of a pair of BK7 glass wedges and chirped mirrors (DCM7 from Venteon (Hannover, Germany), 5 pairs of bounces). As is further detailed below, for different insertions of the wedges, the pulses have different spectral phases and therefore, different durations. At the exit of the compressor, the average light power is around 45 mW and the beam is focused onto the sample using a lens (L1, f = 1 cm). The fluorescence and SHG signals are collected using a microscope objective. To record fluorescence a color filter (FESH0550 from Thorlabs) is

used, while to record the SHG signal color filters Schott BG37 and BG12 are used. Either fluorescence or SHG signals are focused onto a solarized optical fiber (400 μm diameter) using a fused silica lens (L2, f = 5 cm). This fiber is coupled to a UV spectrometer (Ocean Optics HR4000), accumulation times are between 100 and 500 ms at room temperature for both signals. To compare the pulse duration obtained with a standard bulk crystal, the perovskite sample is replaced by a thin BBO crystal (10 μm thickness, cut-off angle 29°). Notice that the sample of Er^{3+}-Ps and the thin BBO crystal are placed in such a way that the laser firstly irradiates the particles or the BBO crystal before passing through the substrate (i.e., the substrate does not affect the pulses before they interact with the Er^{3+} ion, host crystal or the BBO crystal). This implies that there is no difference between the laser pulses which are interacting with the BBO crystal and with the particles.

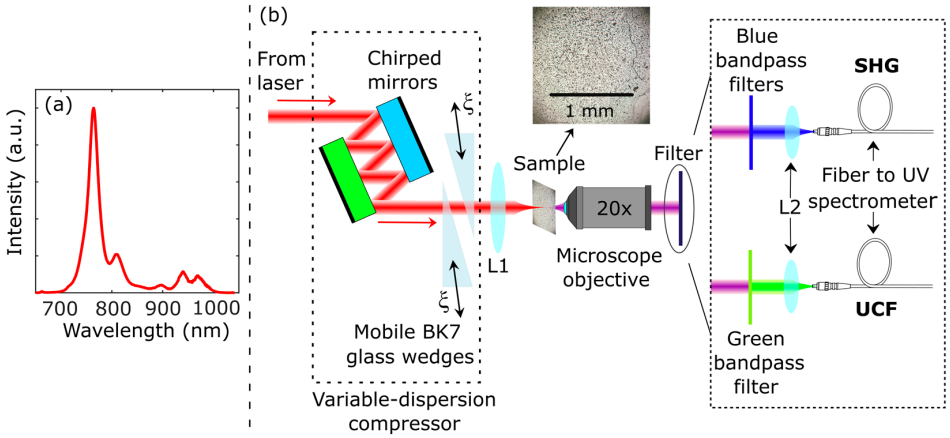

Figure 3. (**a**) Laser spectrum, (**b**) Optical setup. L1, L2 focusing lenses. See text for details.

The operation of a variable dispersion compressor is as follows. Chirped mirrors add a fixed value of negative dispersion per pair of bounces. The positive dispersion can be continuously changed by inserting more or less the wedges in the light path, which changes the total thickness z of glass traversed by the pulse. Bulk SHG crystals, such as BBO (Beta Barium Borate) generate chirp-dependent SHG spectra and this can be used to temporally characterize, both in duration and spectral phase, few-cycle laser pulses. In short, a laser pulse described in the spectral domain as $E(\omega) = \sqrt{I(\omega)}e^{i\phi(\omega)}$ acquires an additional spectral phase when traversing the compressor. To retrieve the pulse it is only necessary to take into account the positive dispersion $k(\omega)z$ added to the pulse when the pulse traverses a certain glass thickness z, which can be changed by inserting the wedges an amount ξ transversally to the light path (Figure 4).

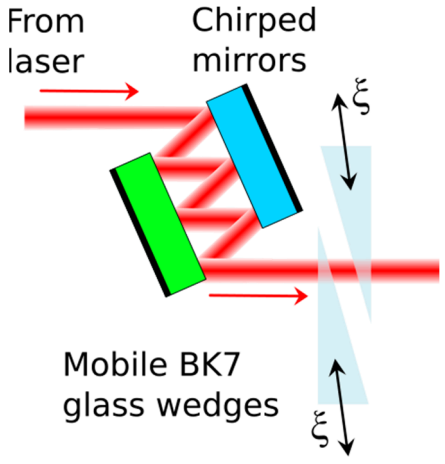

Figure 4. Variable dispersion compressor.

When this pulse generates a SHG signal, the intensity and shape of the spectra change depending on the insertion of the glass wedges and a d-scan trace is recorded as the sequence of SHG spectra as a function of insertion. To retrieve the pulse one simulates the trace that a given pulse would generate when traversing the compressor and compares it with the measured one. The simulated trace is given by [11–13]:

$$S_{sim}(\omega, z) = \left| \int_{-\infty}^{+\infty} \left(\int_{-\infty}^{+\infty} E(\Omega) e^{-ik(\Omega)z} e^{i\Omega t} d\Omega \right)^2 e^{-i\omega t} dt \right|^2 \quad (1)$$

where $k(\omega)z$ is the contribution of the spectral phase associated with the glass thickness z of the glass wedges traversed by the pulse. Therefore, calling $n(\omega)$ the refractive index of the glass and c the velocity of light in vacuum we have $k(\omega) = n(\omega)c/\lambda$, where λ is the wavelength associated with the ω value. The measured trace differs from the theoretical one because of the spectral response of the instrumentation, filters and the SHG material. Therefore, $S_{meas} = R(\omega) \times S_{theo}$. These spectral responses $R(\omega)$ need to be taken into account in the retrieval algorithm. For this purpose, different spectral phases $\phi(\omega)$ are proposed for the laser field and different simulated traces are obtained as a result. These traces are compared to the experimental one in order to calculate the spectral response of the system $\mu(\omega)$ as follows:

$$\mu(\omega) = \mu_i = \frac{\sum_j S_{meas}(\omega_i, z_j) S_{sim}(\omega_i, z_j)}{\sum_j S_{sim}^2(\omega_i, z_j)} \quad (2)$$

being the retrieved trace calculated as $S_{ret} = \mu(\omega) \times S_{sim}$. Note that $R(\omega)$ and $\mu(\omega)$ are conceptually the same function but $R(\omega)$ is related with the experimental response function and does not need to be obtained, while $\mu(\omega)$ is related to the retrieval algorithm and it is calculated at each iteration.

With this information, we can minimize an error function G which measures the difference between the experimental trace and the retrieved trace. This error function G is given by:

$$G = \sqrt{\frac{1}{N_\omega N_z} \sum_{i,j} \left(S_{meas}(\omega_i, z_j) - S_{ret}(\omega_i, z_j) \right)^2} \quad (3)$$

Therefore, $\mu(\omega)$ has the role of encompassing all the spectral responses mentioned above, and can be obtained after the retrieval. In the d-scan technique the pulse is characterized at the focus of the focusing element and it is usually obtained at the compression point, i.e., where the pulse duration is shorter.

In [13,14], we demonstrate that, in order to be able to retrieve the pulse from d-scan traces measured with ensembles of particles it is necessary to take into account an incoherent component in the retrieval algorithm. This incoherent component is caused by the scattering effect in the particles. For this purpose, the final simulated trace is composed of two traces generated by a coherent field ($E_{coh}(\omega)$) and an incoherent field ($E_{incoh}(\omega)$). These two traces are called $S_{coh}(\omega, z)$ and $S_{incoh}(\omega, z)$ respectively. They are weighted by a parameter $X \in [0, 1]$, which we call the coherence factor and contribute as follows to give rise to the total simulated trace:

$$S_{sim}(\omega, z) = X\, S_{coh} + (1 - X)\, S_{incoh} \quad (4)$$

Both traces are generated according to Equation (1) but they differ in the spectral phase of the electric field $E(\omega)$ that generates the trace. For the coherent trace ($S_{coh}(\omega, z)$) the spectral phase of $E_{coh}(\omega)$ is proposed in the same way as in the standard algorithm, while for the incoherent trace ($S_{incoh}(\omega, z)$), the spectral phase of $E_{incoh}(\omega)$ is a random phase that accounts for the scattering suffered by the pulse when passing through the ensemble of particles, and remains fixed during the retrieval process. This retrieval procedure is called

extended algorithm and, with this approach we demonstrated that the incoming pulse can be retrieved despite the scattering [13,14].

3. Results

Figure 5 depicts the SHG signal obtained in BBO and Er^{3+}-Ps for different glass insertions, i.e., different chirps in the laser pulses. As reported in [7], the host of the Er^{3+} ion generates the SHG signal. It is apparent that the SHG spectra change in intensity and shape with the glass insertion, both in the 3D graphs (Figure 5(a1,b1)), and in the top views (Figure 5(a2,b2)). Moreover, both traces are different in shape due to the different non-linear spectral responses of both systems and scattering in the ensemble of Er^{3+}-Ps.

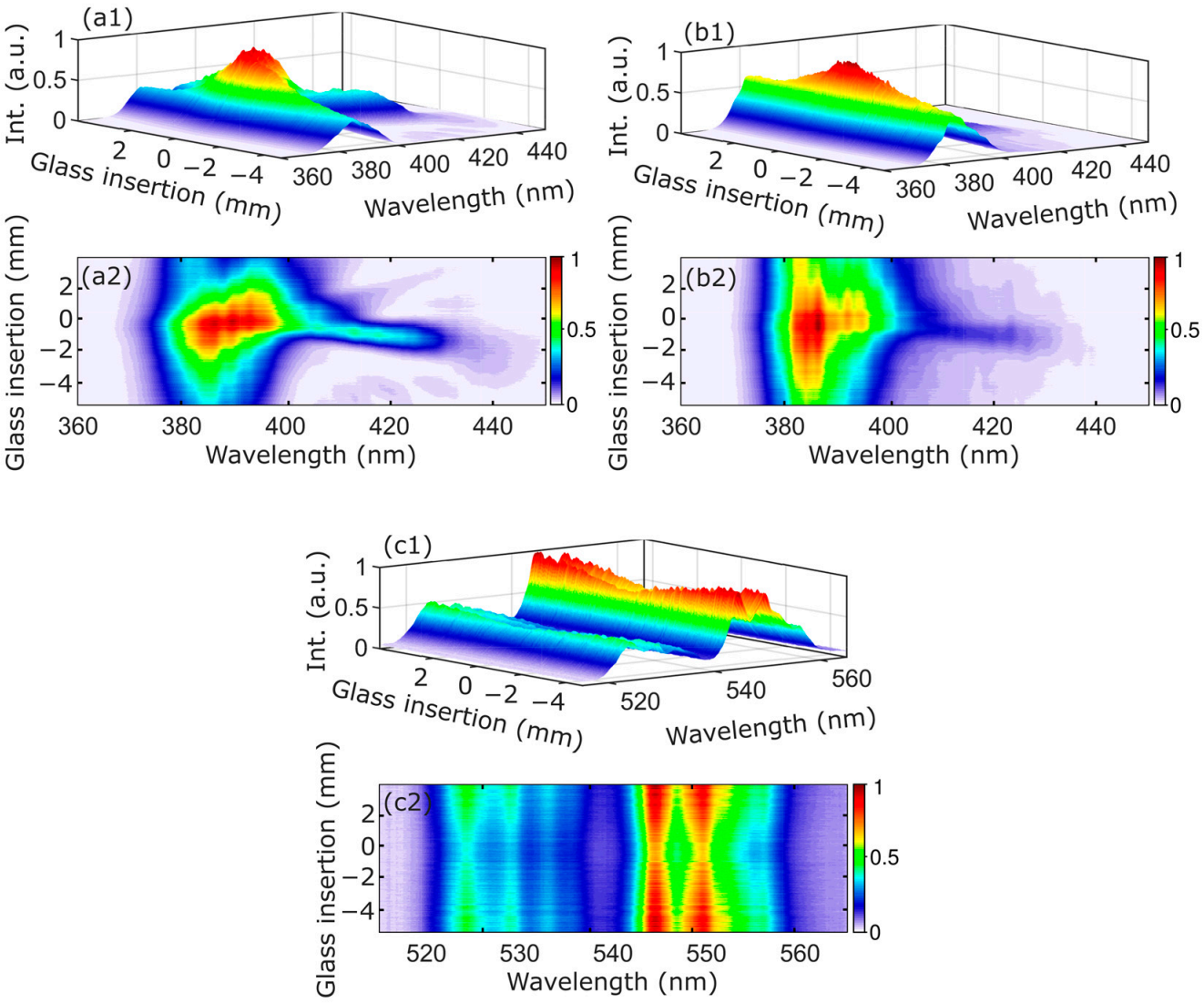

Figure 5. Experimental d-scan traces for SHG signals in BBO (**a1**,**a2**), Er^{3+}-Ps (**b1**,**b2**) and UCF signal in Er^{3+}-Ps (**c1**,**c2**). Upper graphs 3D views (**a1**,**b1**,**c1**); lower graphs (**a2**,**b2**,**c2**) top view of the 3D graphs.

The up-conversion spectra of the Er^{3+}-doped perovskite also change with the chirp of the pulses (Figure 5(c1,c2)). In this case they maintain the band shape, but not the intensity. In particular, we observe a depletion of the fluorescence intensity around glass insertion $z = 0$ mm, i.e., the pulse compression point. The intensity is larger at the extremes of the trace, being the spectrum more intense for approximately $z = +4$ mm than for $z = -4$ mm. This behavior has been previously explained as being due to quantum interference between the levels involved in the UCF signal [7]. The changes in the shape and intensity of both

signals are purely due to the effect of the chirped pulses in the generation of the signals and cannot be attributed to photo-damage. We confirmed this issue by irradiating the samples for around 30 min for different glass-wedges insertions. The signals remained constant during the irradiation time, and no change in the intensity or shape of the spectrum was observed.

Therefore, knowing the temporal characteristics of the laser pulse that produces the excitation of the UCF signal is of key importance.

In this way, due to the dual-emission property of the Er^{3+}-doped perovskite it is possible to retrieve in-situ the laser pulse which is producing the chirp-dependent UCF.

Figure 6(a1,b1) show the d-scan traces retrieved with a BBO crystal and with Er^{3+}-Ps, with the standard and extended algorithm, respectively. Figure 6(a2,b2) show the linear spectrum of the pulse along with the retrieved spectral phase. Both systems retrieve the same spectral phase at the compression point (z = 0 mm) in the zones where the laser spectrum has non-zero intensity. Figure 6(a3,b3) show the retrieved pulse duration at the compression point (z = 0 mm). Both systems retrieve a 7.6 fs pulse duration, and the pulse has the same structure, with a pre-pulse at approximately -15 fs. Note the differences in shape between the two traces due to, on one side, the scattering component which is present in the trace measured with Er^{3+}-Ps and, on the other side, the different spectral responses of the nonlinear media. In spite of these factors and thanks to the extended retrieval procedure and the calculation of the spectral response $\mu(\omega)$ within the algorithm, in both cases we achieve successful retrievals. For these two retrievals, the error function G gives values below the threshold that we set to identify a good retrieval ($G < 0.03$).

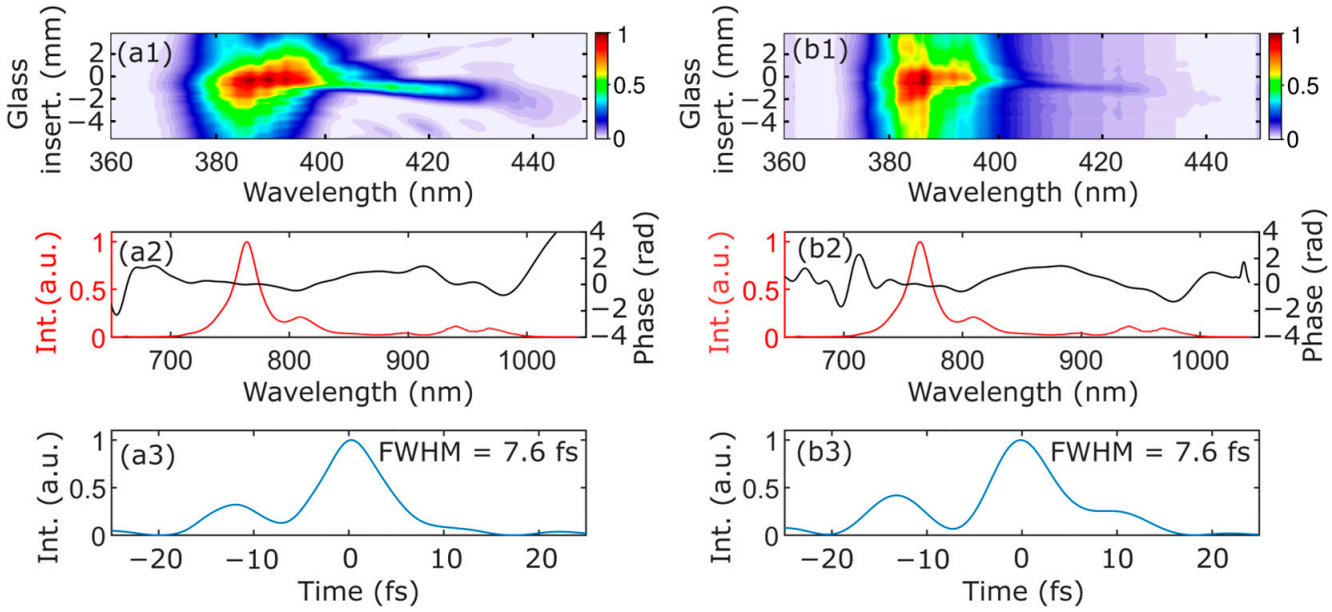

Figure 6. Retrieved d-scan traces in BBO and Er^{3+}-Ps (**a1**,**b1**). Laser spectrum and spectral phases at compression in BBO and Er^{3+}-Ps (**a2**,**b2**). Retrieved pulses at compression in BBO and Er^{3+}-Ps (**a3**,**b3**).

These results validate the host of our Er^{3+}-Ps as an adequate medium to temporally characterize ultrabroad-band laser pulses. This means that, in spite of having the simultaneous emission of a UCF signal, we can measure in-situ the temporal characteristics of the laser pulses that are exciting the up-conversion signal for each insertion/dispersion value. This is depicted in Figure 7, where a sequence of pulses measured with BBO and Er^{3+}-Ps for different glass insertions is represented, along with the fluorescence signal generated for each excitation situation.

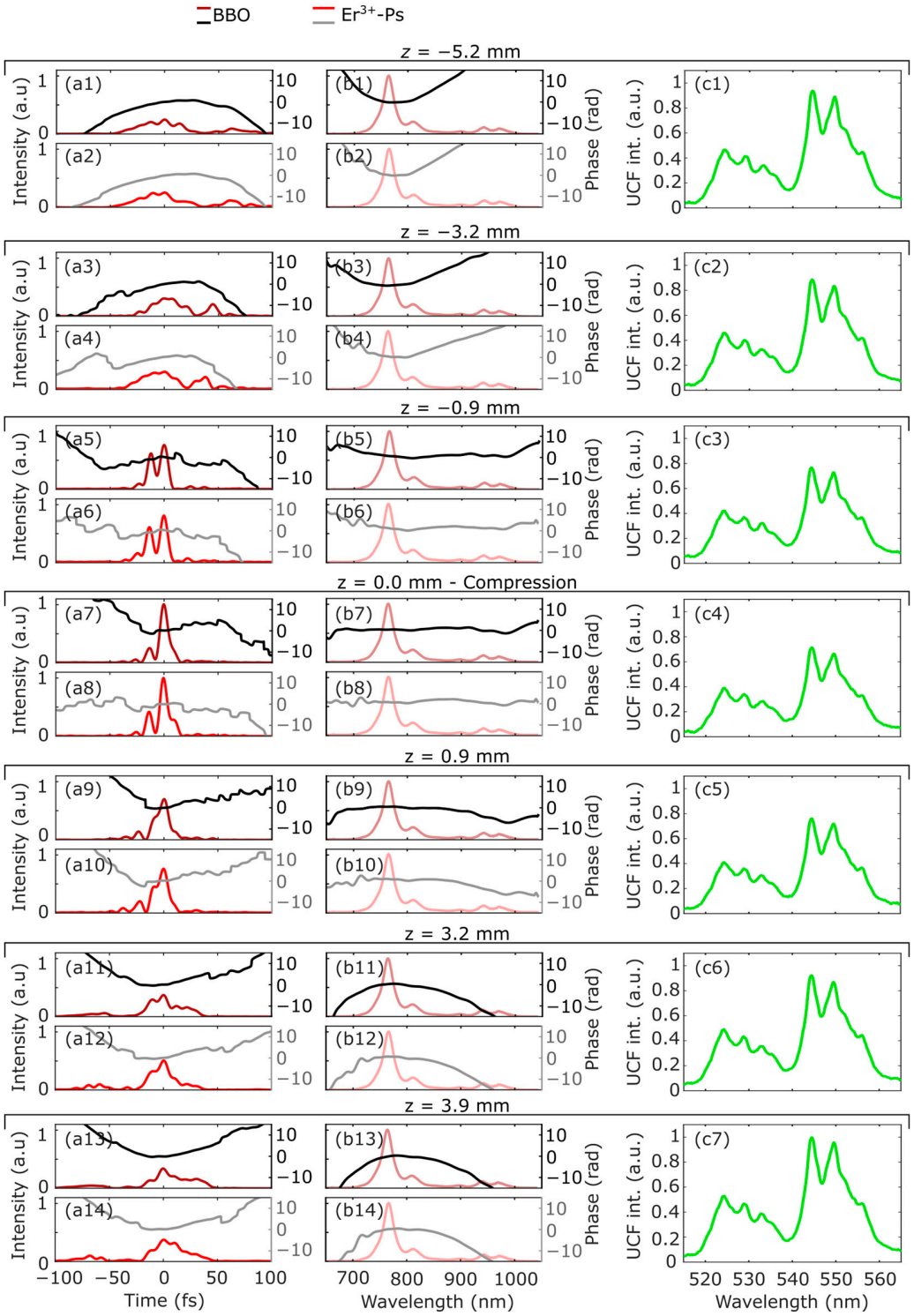

Figure 7. Retrieved exciting laser pulses and retrieved temporal phases for different wedge insertions (**a1**–**a14**): using BBO (pulse in dark red and phase in black) and using Er^{3+}-Ps (pulse in bright red and phase in grey). Measured laser spectrum and retrieved spectral phases for the same wedge insertions (**b1**–**b14**): using BBO (spectrum in dark red, opacity level at 40% and phase in black) and using Er^{3+}-Ps (spectrum in bright red, opacity level at 40% and phase in grey). Measured up-conversion fluorescence spectra for the same wedge insertions (**c1**–**c7**). Insertion z = 0 mm corresponds to the compressed pulse.

In the left column we depict the temporal pulse shape along with the retrieved temporal phase obtained from the traces measured with BBO or Er^{3+}-Ps for different glass

insertions. The pulse durations, calculated as full width half maximum, range from ∼45 fs in the extremes of the trace to ∼8 fs in the compression point. In the central column we display the measured linear spectrum of the laser and the retrieved spectral phases obtained from the traces measured with BBO or Er^{3+}-Ps for the same glass insertions as before. In all cases (b1 to b14) the laser spectrum is exactly the same, since it is a direct measurement. We highlight this to ease the comparison of spectral phases between the different cases in relation to the spectral laser intensity. The colors selected are identical to those employed for the pulses in the left column, but they are set at a 40% opacity level to avoid excessive highlighting. In the right column, the fluorescence spectra of the Er^{3+} ion are depicted. The most intense one (c7) is normalized to unity, and the rest refer to it. As in Figure 5, we see that different glass insertions, i.e., different chirps in the pulses generate fluorescence with different intensities. For $z = 0.0$ mm the spectral phase is essentially flat, and the fluorescence intensity is the lowest one. For positive chirp, the fluorescence intensity increases progressively until reaching a maximum for $z = 3.9$ mm. For negative chirp, the fluorescence also increases progressively up to $z = -5.2$ mm, but the maximum reached is not as high as for the cases of positive chirp. This can also be clearly seen when comparing the cases $z = -0.9, +0.9$ mm and $z = -3.2, +3.2$ mm. In [7] we explain this behavior as being due to pulse coherent effects. Therefore, although the pulse durations can be the same, the chirp of the pulse can be different and can influence how the upper levels $^4I_{9/2}$ and $^4H_{9/2}$ are populated and as a consequence, influence the behavior of the fluorescence emission. Therefore, for a profound knowledge of the emission behavior of the Er^{3+} ion the in-situ temporal characterization of the exciting laser pulse is crucial. Notice that the spectral phases retrieved are mainly quadratic in the zones of the spectrum with non-zero intensity. Therefore, with the variable-dispersion compressor, we essentially produce linearly chirped pulses. Moreover, the coincidence of the retrievals for BBO and Er^{3+}-Ps is significant and validates using the host crystal as a medium to characterize in-situ the laser pulses which are inducing UCF in the Er^{3+}-ion.

It is important to note that, if one uses a different and thicker bulk crystal to measure the laser pulses, it will imprint an additional amount of dispersion to the pulses. For this reason, the pulse measured with a thick bulk crystal is not adequately characterized and it is not a correct retrieval for the pulse that is actually interacting with the Er^{3+} ion. Since we use a 10 µm- thick crystal, we do not notice such a difference. Instead, the in-situ measurement of the laser pulses by taking advantage of the SH signal produced by the host perovskite completely avoids this issue.

4. Conclusions

We have demonstrated that the host of a fluorescent ion can be used as a nonlinear medium to in-situ temporally characterize the ultrashort laser pulses that are exciting the ion fluorescence. That is, the characterization takes place at the same point where the laser is exciting the fluorescence emission. This allows us to avoid changing the optical setup in order to characterize the incoming laser pulse, easing the procedure and reducing the experimental error. This is of great importance when studying the coherence effects induced by a laser pulse on the fluorescent system.

As long as the host generates SHG, this procedure can be employed when using a broadband laser as the exciting source.

Author Contributions: Conceptualization, R.W.; methodology, R.W.; software, Ó.P.-B.; validation, Ó.P.-B. and R.W.; formal analysis, Ó.P.-B.; investigation Ó.P.-B. and R.W.; resources, R.W.; data curation, Ó.P.-B.; writing—original draft preparation, R.W. and Ó.P.-B.; writing—review and editing, R.W. and Ó.P.-B.; visualization Ó.P.-B. and R.W.; supervision R.W.; project administration, R.W.; funding acquisition R.W. All authors have read and agreed to the published version of the manuscript.

Funding: This research was funded by the Spanish MINECO, grant number FIS2017-87360-P. Óscar Pérez-Benito acknowledges a predoctoral contract from UCM (call CT63/19-CT64/19).

Institutional Review Board Statement: Not applicable.

Informed Consent Statement: Not applicable.

Data Availability Statement: The data are available upon reasonable request.

Acknowledgments: We acknowledge our colleagues Susana García-Martín and Ester García-González for the synthesis and characterization of the particles used in this work.

Conflicts of Interest: The authors declare no conflict of interest.

References

1. Jaque, D.; Richard, C.; Viana, B.; Soga, K.; Liu, X.; Sole, J.G. Inorganic nanoparticles for optical bioimaging. *Adv. Opt. Photonics* **2016**, *8*, 1–103. [CrossRef]
2. Liu, Y.; Tu, D.; Zhu, H.; Chen, X. Lanthanide-doped luminescent nanoprobes: Controlled synthesis, optical spectroscopy, and bioapplications. *Chem. Soc. Rev.* **2013**, *42*, 6924–6958. [CrossRef] [PubMed]
3. Chen, G.; Qiu, H.; Prasad, P.N.; Chen, X. Upconversion nanoparticles: Design, nanochemistry, and applications in theranostics. *Chem. Rev.* **2014**, *114*, 5161–5214. [CrossRef] [PubMed]
4. Bonacina, L.; Brevet, P.-F.; Finazzi, M.; Celebrano, M. Harmonic generation at the nanoscale. *J. Appl. Phys.* **2020**, *127*, 230901. [CrossRef]
5. Mayer, L.; Dantelle, G.; Jacques, V.; Perruchas, S.; Patriarche, G.; Roch, J.-F.; Gacoin, T. Dual light-emitting nanoparticles: Second harmonic generation combined with rare-earth photoluminescence. *J. Mater. Chem. C* **2014**, *2*, 7681–7686. [CrossRef]
6. Regny, S.; Riporto, J.; Mugnier, Y.; Le Dantec, R.; Kodjikian, S.; Pairis, S.; Gautier-Luneau, I.; Dantelle, G. Microwave synthesis and up-conversion properties of SHG-active α-(La, Er)$(IO_3)_3$ Nanocrystals. *Inorg. Chem.* **2019**, *58*, 1647–1656. [CrossRef] [PubMed]
7. Pérez-Benito, Ó.; Antón, M.Á.; Urones-Garrote, E.; García-Martín, S.; García-González, E.; Weigand, R. Chirp-dependent dual light emission in $Na_{0.95}Er_{0.05}Nb_{0.9}Ti_{0.1}O_3$ perovskite. *Opt. Mater.* **2022**, *129*, 112500. [CrossRef]
8. Liang, X.; Hu, W.; Fu, L. Pulse compression in two-photon excitation fluorescence microscopy. *Opt. Express* **2010**, *18*, 14893–14904. [CrossRef] [PubMed]
9. Nag, A.; Goswami, D. Effect of linear chirp on femtosecond two-photon processes in solution. *J. Spectrosc. Dyn.* **2012**, *2*, 11. [PubMed]
10. Yakovlev, V.V.; Bardeen, C.J.; Che, J.; Cao, J.; Wilson, K.R. Chirped pulse enhancement of multiphoton absorption in molecular iodine. *J. Chem. Phys.* **1998**, *108*, 2309–2313. [CrossRef]
11. Miranda, M.; Fordell, T.; Arnold, C.; L'Huillier, A.; Crespo, H. Simultaneous compression and characterization of ultrashort laser pulses using chirped mirrors and glass wedges. *Opt. Express* **2012**, *20*, 688–697. [CrossRef] [PubMed]
12. Miranda, M.; Arnold, C.L.; Fordell, T.; Silva, F.; Alonso, B.; Weigand, R.; L'Huillier, A.; Crespo, H. Characterization of broadband few-cycle laser pulses with the d-scan technique. *Opt. Express* **2012**, *20*, 18732–18743. [CrossRef] [PubMed]
13. Pérez-Benito, Ó.; Weigand, R. Nano–dispersion–scan: Measurement of sub-7-fs laser pulses using second-harmonic nanoparticles. *Opt. Lett.* **2019**, *44*, 4921–4924. [CrossRef] [PubMed]
14. Pérez-Benito, Ó.; Cabrera-Granado, E.; García-Martín, S.; García-González, E.; Weigand, R. On the generality of measuring ultrabroad-band ultrashort laser pulses with the d-scan technique using ensembles of dielectric nano-and microparticles. *Opt. Laser Technol.* **2023**, *168*, 109841. [CrossRef]